

Understanding the Photophysics of the Spinach–DFHBI RNA Aptamer–Fluorogen Complex To Improve Live-Cell RNA Imaging

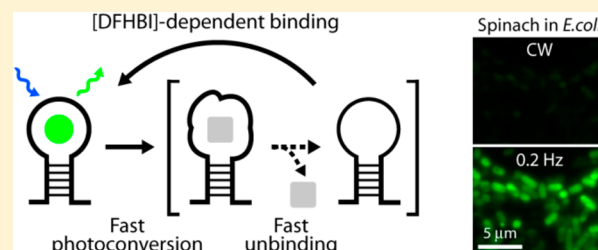
Kyu Young Han,^{†,‡} Benjamin J. Leslie,^{†,‡} Jingyi Fei,[‡] Jichuan Zhang,[§] and Taekjip Ha^{*,†,‡,||}

[†]Howard Hughes Medical Institute, Urbana, Illinois 61801, United States

[‡]Department of Physics and Center for the Physics of Living Cells, [§]Department of Materials Science and Engineering, and ^{||}Institute for Genomic Biology, University of Illinois at Urbana-Champaign, Urbana, Illinois 61801, United States

S Supporting Information

ABSTRACT: The use of aptamer–fluorogen complexes is an emerging strategy for RNA imaging. Despite its promise for cellular imaging and sensing, the low fluorescence intensity of the Spinach–DFHBI RNA aptamer–fluorogen complex hampers its utility in quantitative live-cell and high-resolution imaging applications. Here we report that illumination of the Spinach–fluorogen complex induces photoconversion and subsequently fluorogen dissociation, leading to fast fluorescence decay and fluorogen-concentration-dependent recovery. The fluorescence lifetime of Spinach–DFHBI is 4.0 ± 0.1 ns irrespective of the extent of photoconversion. We detail a low-repetition-rate illumination scheme that enables us to maximize the potential of the Spinach–DFHBI RNA imaging tag in living cells.



INTRODUCTION

RNA has important roles in various cellular and developmental processes. It not only functions as a passive intermediary in protein production based on genetic information but also is a post-transcriptional regulator of gene expression.¹ Fluorescence imaging is one of the most valuable tools for studying these diverse functions of RNA by enabling direct visualization of RNA molecules in the cell and providing temporal and spatial information.² For example, it has been used to characterize transcription, transport, localization, translation, and degradation of messenger RNA³ and to reveal critical roles played by noncoding RNA.⁴

Several RNA-imaging techniques have been developed, of which the most widely used are fluorescence in situ hybridization (FISH) with organic-dye-labeled oligonucleotide probes in fixed cells⁵ and fluorescent-protein-fused RNA binding proteins in living cells.^{6–8} In particular, the MS2 system has been widely used for in vivo labeling of transcripts containing repeated stem–loops, which are specifically bound by a coat protein of bacteriophage MS2 fused to a green fluorescent protein (GFP).⁶ Each of these two techniques has a key limitation of its utility. RNA FISH has single-RNA sensitivity but is largely limited to fixed cells. MS2 systems can be used in live cells, but high background fluorescence from unbound GFP limits their sensitivity. So-called “split-GFP” approaches significantly decrease the background signal,^{8,9} but at a considerable cost to the fluorescence intensity of assembled GFP fluorophores.¹⁰ While these techniques are complementary, a single technique that combines the sensitivity of FISH with live-cell capabilities would be valuable.

Recently, a simple and powerful method was introduced that facilitates RNA detection. A nontoxic and membrane-permeable nonfluorescent GFP chromophore analogue (or fluorogen), 3,5-difluoro-4-hydroxybenzylidene imidazolinone (DFHBI), binds to a genetically encoded RNA aptamer called “Spinach,” eliciting green fluorescence (Figure 1a).¹¹ Indeed, Spinach was successfully implemented for visualization of ribosomal RNA in living mammalian cells¹¹ and sensing of intracellular metabolites and protein expression by means of modular aptamers.¹² This fluorescent tag motivates potential applications to quantitative imaging of low-abundance RNA targets.

Under cellular imaging conditions, however, Spinach shows greatly reduced fluorescence compared with what is expected on the basis of its nominal brightness, which is reported to be similar to that of GFP.^{11,13} Here we present a plausible mechanism to explain its limited fluorescence intensity and show that this aptamer–fluorogen complex has novel properties distinct from typical fluorescent proteins. Exploiting its underlying photophysical properties, we demonstrate that >5-fold higher total photon flux and 10-fold higher steady-state fluorescence intensity can be obtained by low-repetition-rate illumination in living *Escherichia coli*.

MATERIALS AND METHODS

Chemical Synthesis of DFHBI. DFHBI was synthesized from 4-hydroxy-3,5-difluorobenzaldehyde as a starting reagent following the

Received: October 29, 2013

Published: November 28, 2013

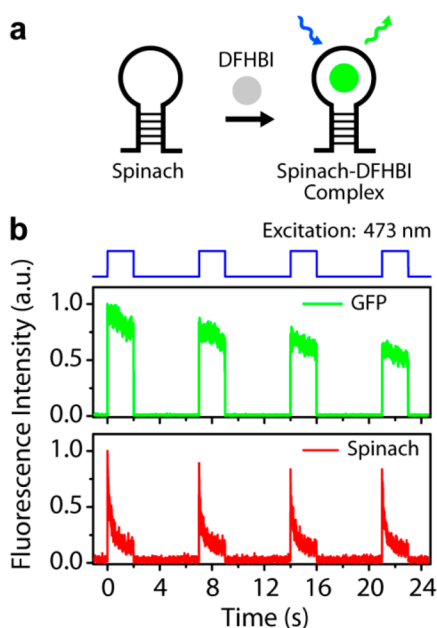


Figure 1. (a) The binding of the GFP-like fluorogen DFHBI to the RNA aptamer Spinach activates green fluorescence upon 473 nm illumination. (b) Fluorescence time traces of GFP (green) and Spinach (red) immobilized on a surface and subjected to light that was turned on and off periodically (blue, $I_{\text{exc}} = 0.2 \text{ kW/cm}^2$). The Spinach–DFHBI complex shows fast fluorescence decay and reversible recovery in the dark, whereas GFP displays irreversible fluorescence decay on this time scale.

procedure of Paige and co-workers [see the Supporting Information (SI) for details].¹¹

Preparation of the Spinach RNA Aptamer. DNA coding for the Spinach aptamer was cloned into the pET28a plasmid (Novagen). Spinach was subsequently transcribed *in vitro* from the T7 promoter using a MEGAshortscript T7 Kit (Ambion) according to the protocol provided by the manufacturer. Then the transcribed RNA was buffer-exchanged with a Micro Bio-Spin P-6 column (Bio-Rad) three times into storage buffer (10 mM Tris-HCl, pH 7.5, 0.1 mM EDTA, and 10 mM KCl) to remove free, unincorporated nucleotides. The Spinach RNA was then folded in 40 mM HEPES buffer (pH 7.5) with 125 mM KCl by incubation at 90 °C for 2 min and slow cooling to room temperature. At 65 °C, MgCl₂ was supplemented to a final concentration of 5 mM, and cooling was resumed.¹¹ For experiments requiring attachment of Spinach to surfaces, a biotin-labeled DNA oligonucleotide (5'-TTATCCGCTCACAATTCATTTG-biotin-3', Integrated DNA Technologies) was annealed to the Spinach 5'-end by direct mixing of the biotin–DNA with Spinach during folding as described above.

Surface Immobilization of GFP and Spinach. A flow chamber was prepared on a poly(ethylene glycol) (PEG)-coated coverslip with a low density of biotin–PEG (Laysan Bio).¹⁴ Neutravidin (0.2 mg/mL, Thermo Scientific) was incubated for 5 min and washed away with 1× PBS buffer (Lonza no. 17-517Q). Freshly folded biotinylated Spinach aptamer (10 nM) was incubated for 10 min in an imaging buffer consisting of 40 mM HEPES (pH 7.5) with 125 mM KCl and 5 mM MgCl₂.¹¹ Then various concentrations of DFHBI (50 μL) in the same buffer were loaded to the chamber for the measurements. The surface density of the immobilized RNA was roughly 5–20 molecules per focal volume. In the case of fluorescent proteins, recombinant *Aequorea coerulescens* GFP (rAcGFP1) was purchased from Clontech and used without further purification. The spectral properties of rAcGFP1 (hereinafter simply GFP) are reported to be similar to those of enhanced GFP.¹⁵ To immobilize GFP to the PEG surface, a biotinylated rabbit polyclonal anti-GFP antibody (Rockland Immunochemicals) was incubated on Neutravidin-coated flow chambers for

5 min and then washed out. After incubation of GFP (5 nM) in the flow chamber for 10 min, unbound excess proteins were flushed before measurements were taken.

Fluorescence Intensity and Lifetime Measurements. We used a custom-built confocal microscope to detect fluorescence of GFP and Spinach, unless specified otherwise.¹⁶ A blue diode laser (473 nm, CNI laser) was used to illuminate the sample, and the illumination time and level of light intensity were controlled by acousto-optical filters (MT200-A0.5-VIS, AA Opto-Electronic). The fluorescence lifetime measurements were performed using the same microscope with an ultrafast laser (MaiTai HP, Spectra Physics) and a time-correlated single photon counting module (SPC630, Becker Hickl).¹⁷ Please refer to the SI for more information.

Binding and Unbinding Kinetics Measurements. The fluorescence increase was recorded with a fluorometer (Cary Eclipse) after rapid mixing of 40 nM Spinach with different concentrations of DFHBI in a cuvette (80 μL). The excitation and emission wavelengths were 460 and 510 nm, respectively. The illumination intensity was estimated to be 1–5 W/cm². The fluorescence intensity followed a single-exponential time course.

Live-Cell Imaging in *E. coli*. Rosetta (DE3) competent cells (Novagen) were transformed with pET28c-tRNA-Spinach (provided by Prof. Samie Jaffrey), which encodes a Spinach aptamer inserted into the tRNA^{Lys3} sequence. Cultures were grown overnight with shaking in Luria Broth (LB) containing 50 μg/mL kanamycin at 37 °C. Then aliquots of the static culture were added to 5 mL of LB containing 1 mM isopropyl β-D-1-thiogalactopyranoside (IPTG) to reach an optical density of 0.4 at 600 nm and induced at 37 °C. After 2.5 h, 100 μL aliquots of cells were added to individual wells of an eight-well Lab-Tek chamber (NUNC no. 155411) coated with polylysine, and cells were allowed to adhere for 30 min at 25 °C. Cell-coated surfaces were gently washed two times with 200 μL of modified minimal M9CA broth (Teknova no. M8011) with glycerol supplemented with 1 mM IPTG and then incubated for 30 min at 25 °C in 200 μL of M9CA containing 1 mM IPTG and 100 μM DFHBI. We used a home-built epi-illumination microscope to image live cells with an oil immersion objective lens (NA = 1.4, UPlanSApo 100×, Olympus) and an EMCCD camera (iXon DU-897, Andor). The illumination time of 473 nm light was synchronized to clock signals of the camera and controlled by a custom program. Image analysis was performed using MATLAB (The MathWorks) and ImageJ (NIH) software.

RESULTS AND DISCUSSION

Fast Fluorescence Intensity Decay and Recovery of the Spinach–DFHBI Complex. Figure 1b shows typical fluorescence intensity time traces of the surface-immobilized fluorescent protein and Spinach at high-density coverage under a focused laser beam. While blue laser light (473 nm) with an excitation intensity (I_{exc}) of 0.2 kW/cm² was periodically turned on and off, the fluorescence signal was monitored by confocal microscopy at room temperature. As expected, the fluorescence intensity of GFP decreased slowly and did not recover in subsequent pulses. It is well-known that GFP's signal drop comes from irreversible photobleaching¹⁸ and/or photo-conversion to a long-lived dark state.¹⁹

In contrast, when the same excitation scheme was applied to Spinach in the presence of excess DFHBI (5 μM), the initially bright fluorescence of the Spinach–DFHBI complex showed fast decay to a significantly reduced fluorescence level (<5% of the initial level) within 2 s. Remarkably, after the excitation light was switched off for a few seconds, a subsequent pulse revealed that the fluorescence signal was recovered back to 85–95% of the initial signal. This indicates that the fluorescence loss of Spinach–DFHBI is not due to fast, irreversible photobleaching but instead is caused by reversible conversion to a non-fluorescent state and that the signal recovery occurs spontaneously without light.

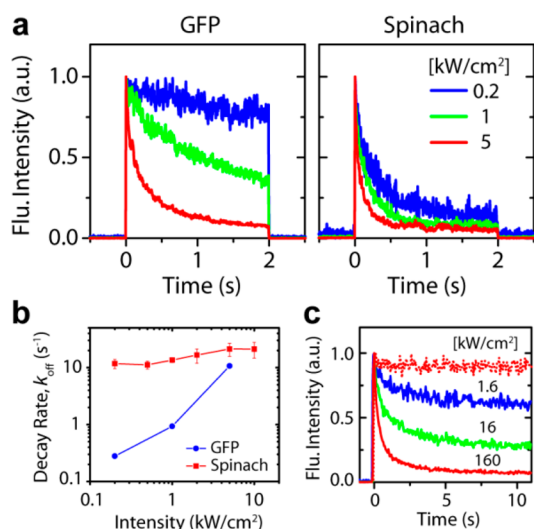


Figure 2. (a) Fluorescence time traces and (b) decay rates of immobilized GFP and Spinach–DFHBI complex as a function of I_{exc} . The fluorescence intensity is normalized to the maximum value at the highest I_{exc} and the decay rate (k_{off}) is the inverse of the half-life. $[\text{DFHBI}] = 5 \mu\text{M}$. (c) Fluorescence intensity time traces of Spinach free in solution (solid lines). The red dotted line is for GFP free in solution at $I_{\text{exc}} = 160 \text{ kW/cm}^2$.

Power-Dependent Fluorescence Decay. We next examined how the excitation intensity I_{exc} affects the fluorescence decay (Figure 2a). The fluorescence decay of GFP becomes faster at higher I_{exc} , and its decay rate (k_{off}) increases linearly with I_{exc} (Figure 2b). For Spinach, however, k_{off} exhibits a weaker dependence on I_{exc} : it changes only 2-fold (from 11.7 to 21.2 s^{-1}) when I_{exc} increases 25-fold from 0.2 to 5 kW/cm^2 , a range of I_{exc} commonly used in confocal microscopy and single-molecule imaging (Figure 2b). The very weak dependence of the fluorescence decay rate on I_{exc} suggests that fluorescence loss requires at least two steps, an initial light-dependent step already saturated at our typical I_{exc} values and a second light-independent step.

For the free species in solution, the fluorescence decay would be difficult to detect because of replenishment of fluorescently active species from outside the excitation volume via diffusion. This was indeed the case for GFP (Figure 2c). For Spinach–DFHBI, however, photoconversion is very efficient, saturating even at moderate I_{exc} values (Figure 2a), and as a result, we could observe significant fluorescence decays even without immobilization (Figure 2c). To achieve the same degree of fluorescence decay for GFP, we had to use 1000 times higher I_{exc} (Figure 2c and Figure S1 in the SI). This set of measurements on free species in solution further indicates that the weak I_{exc} dependence of the fluorescence decay kinetics of immobilized Spinach–DFHBI is due to saturation of the highly efficient photoconversion process (please see the SI for further discussion).

Fluorescence Lifetime of the Spinach–DFHBI Complex. We examined the time-resolved fluorescence of the Spinach–DFHBI complex in two different ways to gain further insights. First, the fluorescence lifetime (τ_f) was measured when >80% of the complex was photoconverted after 8 s of illumination (Figure 3, top left). Second, τ_f was measured during a 20 ms pulse of illumination time every 2 s to ensure collection of the fluorescence mainly from the bright molecular complex before photoconversion (Figure 3, top right). Here we

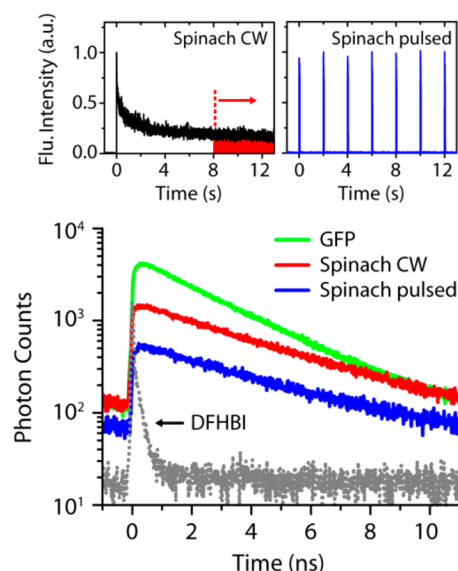


Figure 3. Time-resolved fluorescence of the Spinach–DFHBI complex. The fluorescence lifetime was measured when the degree of photoconversion was maximized (Spinach CW, top left) or minimized (Spinach pulsed, top right). However, both sets of conditions resulted in the same decay rate, $\tau_f = 4.0 \text{ ns}$. For comparison, the decay curves of GFP (green line; $\tau_f = 2.7 \text{ ns}$) and DFHBI-only solution (gray dotted line; $\tau_f < 80 \text{ ps}$) are shown.

used 0.5 μM Spinach and 0.5 μM DFHBI free in solution. As depicted in Figure 3, in both cases (i.e., regardless of the extent of photoconversion), the complex exhibited a single-exponential decay with $\tau_f = 4.0 \pm 0.1 \text{ ns}$, which is 1.5 times longer than that of GFP ($\tau_f = 2.7 \text{ ns}$). This suggests that the photoconverted species does not accumulate to a high degree to be detected based on the fluorescence lifetime. The concentration of DFHBI does not greatly affect the fluorescence lifetime of the Spinach–DFHBI complex (Figure S2 in the SI).

[DFHBI]-Dependent Fluorescence Recovery. These characteristic behaviors of the Spinach–DFHBI complex may be attributed to (i) reversible photoconversion as previously proposed,²⁰ (ii) fluorogen exchange,¹¹ or (iii) a combination of the two. To further clarify the mechanism, we next determined the fluorescence recovery rate as a function of fluorogen concentration. If the Spinach–DFHBI complex is photoconverted to a nonfluorescent state in which the fluorogen is still bound to the RNA aptamer, thermal or light-induced recovery to a fluorescent state would be independent of $[\text{DFHBI}]$. Instead, the recovery rate (k_{on}) displays a strong dependence on $[\text{DFHBI}]$: k_{on} changes from 0.08 to 2.0 s^{-1} as $[\text{DFHBI}]$ increases from 1 to 200 μM (Figure 4). This result is in disagreement with a previous proposal²⁰ where the reported recovery rate was constant at $\sim 0.0027 \text{ s}^{-1}$ independent of the DFHBI concentration. This discrepancy results from the fact that we used immobilized RNA in an excess of DFHBI, whereas in the latter case, the fluorescence recovery measured the replenishment rate of the fluorescent Spinach–DFHBI complex in a freely diffusing solution (please see the SI for detailed discussion). The sublinear behavior of the recovery rate in Figure 4b might be attributed to altered spectral properties of the Spinach–DFHBI complex at high concentrations of DFHBI, although its molecular mechanism remains unclear (Figure S3 in the SI).

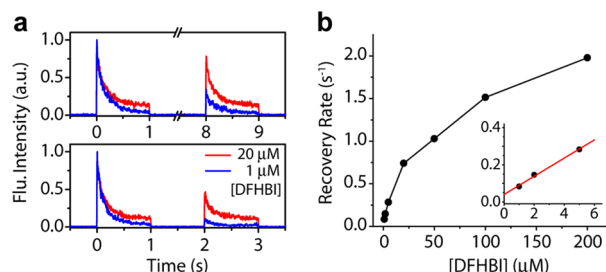


Figure 4. (a) [DFHBI]-dependent fluorescence time traces and (b) recovery rates of the Spinach–DFHBI complex. The inset in (b) shows the recovery rate at low [DFHBI] with a linear fit (red line).

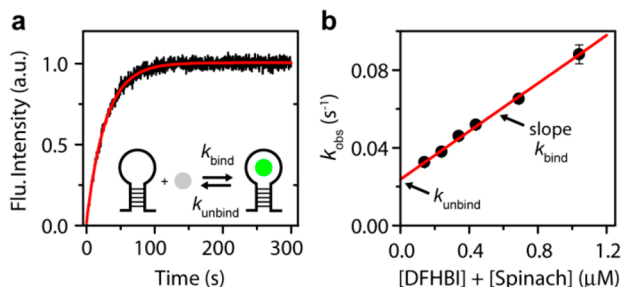


Figure 5. Binding–unbinding kinetics of the Spinach–DFHBI complex. (a) Fluorescence–time profile when 40 nM Spinach was mixed with 200 nM DFHBI under a very low light level. The red line is a monoexponential fit. (b) Determination of the binding (k_{bind}) and unbinding (k_{unbind}) kinetic rates from the linear fit (red solid line) of k_{obs} vs concentration.

Binding–Unbinding Kinetics. Next we examined how fast fluorogen exchange occurs in the Spinach–DFHBI complex. Spinach RNA was mixed with DFHBI in a quartz cuvette, and the fluorescence change was monitored at a very low light level (<1 to 5 W/cm^2) to minimize complications arising from photoconversion. Figure 5a shows that the fluorescence signal rises monoexponentially, giving the observed rate constant (k_{obs}). The slope of the linear fit of the plot of k_{obs} versus the concentration of Spinach and DFHBI (Figure 5b) directly provides the binding rate constant, k_{bind} , and intercept gives the unbinding rate constant, k_{unbind} . The obtained values, $k_{\text{bind}} = (6.2 \pm 0.1) \times 10^4 \text{ M}^{-1} \text{ s}^{-1}$ and $k_{\text{unbind}} = (2.4 \pm 0.1) \times 10^{-2} \text{ s}^{-1}$, yield a dissociation equilibrium constant $K_{\text{D}} = 390 \text{ nM}$, which is in good agreement with previous studies.^{11,20} Here, k_{bind} of Spinach–DFHBI is well within the range of typical small-molecule–RNA aptamer interactions, which vary from 10^3 to $10^6 \text{ M}^{-1} \text{ s}^{-1}$.²¹

It should be noted that the dissociation time ($1/k_{\text{unbind}}$) is very long, and therefore, once Spinach binds to DFHBI, it stays as a complex for $>40 \text{ s}$ under a low light level or in the absence of light. Also, the [DFHBI] dependence of the recovery rate at low concentrations gives a bimolecular reaction rate of $(4.9 \pm 0.3) \times 10^4 \text{ M}^{-1} \text{ s}^{-1}$, which corresponds well to k_{bind} (Figure 4b inset). This confirms that the fluorescence recovery is mainly due to a bimolecular reaction between Spinach and DFHBI rather than a spontaneous recovery of the photoconverted complex.

Fluorescence Signal Gain with Low-Repetition-Rate Illumination and Its Application to *E. coli* Imaging. The limited time duration of the fluorescence of the Spinach–DFHBI can be mitigated by low-repetition-rate illumination. Here the fluorescence intensity was monitored under

continuous-wave (CW) illumination or under pulsed illumination (50 ms pulse width) at a repetition rate varying from 2 to 0.2 Hz (Figure 6a). A similar scheme has been applied in fluorescence microscopy to attain high fluorescence yields from organic dyes and fluorescent proteins, where the repetition rates ranged from 0.1 to 100 kHz to allow dark-state relaxation.²²

To demonstrate the concept, we transformed *E. coli* with plasmids expressing Spinach and imaged them in the presence of $100 \mu\text{M}$ DFHBI (Figure 6b).¹¹ Time-lapse fluorescence microscopy showed that the fluorescence signal of *E. coli* under CW illumination rapidly drops to $<10\%$ of the initial intensity within 0.2 s (Figure 6c), whereas pulsed illumination at a repetition rate of 0.2 Hz retains the fluorescence signal much better by ensuring sufficient recovery time between successive pulses (Figure 6d). This phenomenon holds true for immobilized Spinach RNA aptamers as well (Figure S4 in the SI). We further quantified the data by plotting the fluorescence time trajectories of a single cell (Figure 6e) and 40 cells averaged (Figure 6f).

The accumulated fluorescence intensity, representing the total photon flux, is 5.7-fold higher at 0.2 Hz than with CW illumination for the same 2 s of total illumination time (Figure 6g). The steady-state intensity is about 10-fold higher at 0.2 Hz compared with CW illumination (Figure 6e,f). Although the lower repetition rate gives higher fluorescence signal gain (Figure 6h), there is a trade-off in imaging speed. Different RNA aptamers selected for higher k_{bind} may allow even higher imaging speed. Additionally, pulsed illumination with longer pulse widths is not effective in gaining higher signal and requires more recovery time, probably because shorter pulses (10–50 ms) minimize the photoconversion process (Figure 6i).

Photophysical Model of the Spinach–DFHBI Complex. On the basis of our results, we can rule out the possibilities that Spinach undergoes reversible photoconversion without fluorogen exchange [model (i)] or efficient fluorogen exchange without photoconversion [model (ii)]. A study of a malachite green RNA aptamer has shown that the fluorogen can go through significant changes in its conformation and electronic structure upon illumination.²³ In the case of photoswitchable proteins, photoisomerization is known to be strongly involved with the formation of the dark state,²⁴ where an accompanying change in the configuration of fluorescent proteins leads to the conversion of a (fluorescent) deprotonated state into a (nonfluorescent) protonated state.²⁵ We confirmed that after 405 nm illumination the absorbance of free DFHBI decreases, with its spectrum showing a red-shifted band and an enhanced high-energy band (Figure S5a in the SI). This is very similar to the spectroscopic features of GFP chromophore and its analogues, indicating that cis/trans photoisomerization occurs for DFHBI.²⁶ For these reasons, it is tempting to suggest that the photoconversion of the Spinach–DFHBI complex may also be related to cis/trans photoisomerization, although a definite conclusion should await further studies.^{20,27}

To account for the unique photophysical behavior of Spinach, we propose the alternative model shown in Figure 7. Upon illumination of the Spinach–DFHBI complex, the bound DFHBI undergoes photoisomerization at a high kinetic rate (k_{off}^*). It is possible that the photoisomerized complex before unbinding is already completely dark. However, because of the lifetime measurements shown in Figure 3, we can rule

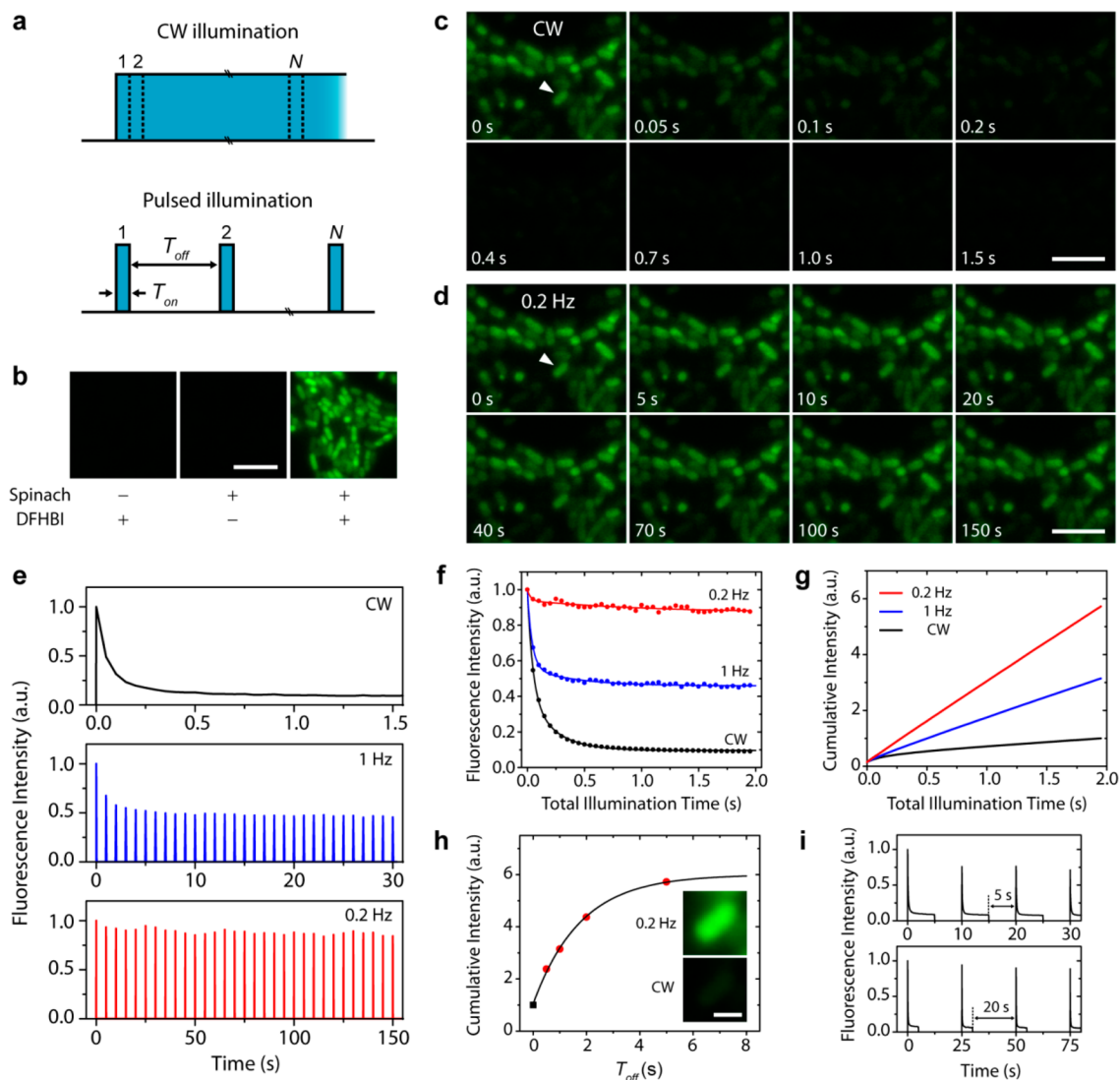


Figure 6. Fluorescence signal gain from living *E. coli* expressing Spinach with low-repetition-rate illumination. (a) Scheme of illumination using CW and pulsed modes. (b) Spinach and DFHBI are necessary for imaging of bright fluorescence from *E. coli*. Scale bar = 5 μm . (c, d) Time-lapse fluorescence images of *E. coli* under (c) CW and (d) pulsed illumination with the same peak intensity (~ 100 W/cm 2). [DFHBI] = 100 μM ; scale bar = 5 μm . (e) Fluorescence intensity traces from the single cell marked by white arrows in (c) and (d). (f) Repetition-rate-dependent fluorescence intensity traces averaged over many cells ($n > 40$). (g) Cumulative fluorescence intensity at various repetition rates. (h) Cumulative fluorescence intensity after 2 s of total illumination time. The CW data point is marked by a black square dot. Inset: Summed images of a single *E. coli* (scale bar = 1 μm). (i) Longer pulse illumination ($T_{on} = 5$ s) leads to less signal gain and longer recovery time.

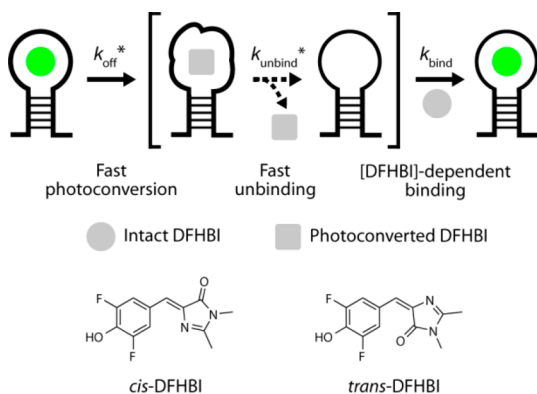


Figure 7. Proposed model of the fluorescence behavior of the Spinach–DFHBI complex. The two isomers of DFHBI are depicted at the bottom.

out the possibility that a partially quenched photoisomerized complex accumulates significantly under our experimental conditions. Photoisomerization results in fast unbinding (k_{unbind}^*) of the photoisomerized fluorogen, in contrast to the long-lived binding of DFHBI under very low or no illumination. Such accelerated unbinding could be caused by two factors: first, since the RNA aptamer was selected on the basis of its binding affinity to the ground-state of DFHBI, its binding affinity to a photoisomerized DFHBI may not be optimal. Second, the Spinach aptamer might also change its conformation to accommodate photoisomerized DFHBI, a phenomenon observed in photoconversion of fluorescent proteins, which could greatly decrease or even abolish binding. Rapid dissociation of photoisomerized DFHBI allows Spinach to bind to a new ground-state DFHBI from solution, restoring the fluorescence. This could also explain why we could not identify the photoisomerized product via fluorescence lifetime

(Figure 3) and the fluorescence excitation spectrum (Figure S5b in the SI). It is also possible that the light-induced fluorescence decay we observed here may be related to the recently reported RNA folding problem of Spinach.²⁸

CONCLUSION

It was reported that the basic fluorescence properties of the Spinach–DFHBI complex are similar to those of enhanced GFP.¹¹ This seems plausible given the similar ways in which the scaffolds of GFP and the Spinach RNA aptamer make a nonfluorescent chromophore fluorescent through structural reinforcement involving specific hydrogen-bonding and π -stacking interactions. However, our results show that the different nature of the RNA aptamer endows unique properties, namely, fast fluorescence decay and [DFHBI]-dependent recovery attributed to photoconversion accompanied by accelerated unbinding. The use of pulsed illumination greatly increases the steady-state fluorescence intensity and total photon flux of the Spinach–DFHBI complex. Combined with signal amplification by attachment of many repeats of the RNA aptamer to a target RNA,²⁹ this pulsed excitation scheme may allow cellular RNA imaging at the single-RNA level with high signal-to-noise ratio. Our study may also provide insights into how to improve the fluorescence properties of the Spinach–DFHBI complex as well as various fluorogenic dye–RNA aptamer complexes.^{29,30}

ASSOCIATED CONTENT

Supporting Information

Experimental details, notes on fluorescence decay in a freely diffusing solution and on the measurement of recovery rates, and Figures S1–S5. This material is available free of charge via the Internet at <http://pubs.acs.org>.

AUTHOR INFORMATION

Corresponding Author

tjha@illinois.edu

Notes

The authors declare no competing financial interest.

ACKNOWLEDGMENTS

We thank Dr. Sung Chul Bae for providing the 473 nm laser and Prof. Samie R. Jaffrey for providing the pET28c-tRNA-Spinach plasmid. Funding was provided by NIH (GM065367 and AI083025) and NSF (PHY0822613). T.H. is an investigator of the Howard Hughes Medical Institute.

REFERENCES

- (1) Krol, J.; Loedige, I.; Filipowicz, W. *Nat. Rev. Genet.* **2010**, *11*, 597. Guttman, M.; Rinn, J. L. *Nature* **2012**, *482*, 339.
- (2) Martin, K. C.; Ephrussi, A. *Cell* **2009**, *136*, 719.
- (3) Moore, M. J. *Science* **2005**, *309*, 1514. Fusco, D.; Accornero, N.; Lavoie, B.; Shenoy, S. M.; Blanchard, J. M.; Singer, R. H.; Bertrand, E. *Curr. Biol.* **2003**, *13*, 161. Shav-Tal, Y.; Darzacq, X.; Shenoy, S. M.; Fusco, D.; Janicki, S. M.; Spector, D. L.; Singer, R. H. *Science* **2004**, *304*, 1797. Golding, I.; Cox, E. C. *Proc. Natl. Acad. Sci. U.S.A.* **2004**, *101*, 11310. Darzacq, X.; Shav-Tal, Y.; de Turris, V.; Brody, Y.; Shenoy, S. M.; Phair, R. D.; Singer, R. H. *Nat. Struct. Mol. Biol.* **2007**, *14*, 796.
- (4) Engreitz, J. M.; Pandya-Jones, A.; McDonel, P.; Shishkin, A.; Sirokman, K.; Surka, C.; Kadri, S.; Xing, J.; Goren, A.; Lander, E. S.; Plath, K.; Guttman, M. *Science* **2013**, *341*, 767.
- (5) Lawrence, J. B.; Singer, R. H.; Marselle, L. M. *Cell* **1989**, *57*, 493. Femino, A.; Fay, F. S.; Fogarty, K.; Singer, R. H. *Science* **1998**, *280*,

585. Raj, A.; van den Bogaard, P.; Rifkin, S. A.; van Oudenaarden, A.; Tyagi, S. *Nat. Methods* **2008**, *5*, 877.

(6) Bertrand, E.; Chartrand, P.; Schaefer, M.; Shenoy, S. M.; Singer, R. H.; Long, R. M. *Mol. Cell* **1998**, *2*, 437.

(7) Daigle, N.; Ellenberg, J. *Nat. Methods* **2007**, *4*, 633.

(8) Ozawa, T.; Natori, Y.; Sato, M.; Umezawa, Y. *Nat. Methods* **2007**, *4*, 413.

(9) Valencia-Burton, M.; McCullough, R. M.; Cantor, C. R.; Broude, N. E. *Nat. Methods* **2007**, *4*, 421.

(10) Kerppola, T. K. *Nat. Rev. Mol. Cell Biol.* **2006**, *7*, 449.

(11) Paige, J. S.; Wu, K. Y.; Jaffrey, S. R. *Science* **2011**, *333*, 642.

(12) Paige, J. S.; Nguyen-Duc, T.; Song, W.; Jaffrey, S. R. *Science* **2012**, *335*, 1194. Song, W.; Strack, R. L.; Jaffrey, S. R. *Nat. Methods* **2013**, *10*, 873.

(13) Strack, R. L.; Jaffrey, S. R. *Curr. Opin. Chem. Biol.* **2013**, *17*, 651.

(14) Roy, R.; Hohng, S.; Ha, T. *Nat. Methods* **2008**, *5*, 507.

(15) Day, R. N.; Davidson, M. W. *Chem. Soc. Rev.* **2009**, *38*, 2887.

(16) Han, K. Y.; Kim, S. K.; Eggeling, C.; Hell, S. W. *Nano Lett.* **2010**, *10*, 3199.

(17) Han, K. Y.; Wildanger, D.; Rittweger, E.; Meijer, J.; Pezzagna, S.; Hell, S. W.; Eggeling, C. *New J. Phys.* **2012**, *14*, No. 123002.

(18) Patterson, G. H.; Knobel, S. M.; Sharif, W. D.; Kain, S. R.; Piston, D. W. *Biophys. J.* **1997**, *73*, 2782.

(19) Dickson, R. M.; Cubitt, A. B.; Tsien, R. Y.; Moerner, W. E. *Nature* **1997**, *388*, 355.

(20) Wang, P.; Querard, J.; Maurin, S.; Nath, S. S.; Le Saux, T.; Gautier, A.; Jullien, L. *Chem. Sci.* **2013**, *4*, 2865.

(21) Kulshina, N.; Baird, N. J.; Ferre-D'Amare, A. R. *Nat. Struct. Mol. Biol.* **2009**, *16*, 1212. Wang, T. J.; Hoy, J. A.; Lamm, M. H.; Nilsen-Hamilton, M. *J. Am. Chem. Soc.* **2009**, *131*, 14747.

(22) Donnert, G.; Eggeling, C.; Hell, S. W. *Nat. Methods* **2007**, *4*, 81. Dean, K. M.; Lubbeck, J. L.; Binder, J. K.; Schwall, L. R.; Jimenez, R.; Palmer, A. E. *Biophys. J.* **2011**, *101*, 961.

(23) Nguyen, D. H.; DeFina, S. C.; Fink, W. H.; Dieckmann, T. J. *Am. Chem. Soc.* **2002**, *124*, 15081.

(24) Chudakov, D. M.; Feofanov, A. V.; Mudriku, N. N.; Lukyanov, S.; Lukyanov, K. A. *J. Biol. Chem.* **2003**, *278*, 7215. Andresen, M.; Stiel, A. C.; Trowitzsch, S.; Weber, G.; Eggeling, C.; Wahl, M. C.; Hell, S. W.; Jakobs, S. *Proc. Natl. Acad. Sci. U.S.A.* **2007**, *104*, 13005.

(25) Tolbert, L. M.; Baldrige, A.; Kowalik, J.; Solntsev, K. M. *Acc. Chem. Res.* **2012**, *45*, 171. Dedecker, P.; De Schryver, F. C.; Hofkens, J. *J. Am. Chem. Soc.* **2013**, *135*, 2387.

(26) Voliani, V.; Bizzarri, R.; Nifosi, R.; Abbruzzetti, S.; Grandi, E.; Viappiani, C.; Beltram, F. *J. Phys. Chem. B* **2008**, *112*, 10714.

(27) Addison, K.; Conyard, J.; Dixon, T.; Page, P. C. B.; Solntsev, K. M.; Meech, S. R. *J. Phys. Chem. Lett.* **2012**, *3*, 2298.

(28) Strack, R. L.; Disney, M. D.; Jaffrey, S. R. *Nat. Methods* **2013**, *10*, 1219.

(29) Babendure, J. R.; Adams, S. R.; Tsien, R. Y. *J. Am. Chem. Soc.* **2003**, *125*, 14716.

(30) Sparano, B. A.; Koide, K. *J. Am. Chem. Soc.* **2007**, *129*, 4785. Constantin, T. P.; Silva, G. L.; Robertson, K. L.; Hamilton, T. P.; Fague, K.; Waggoner, A. S.; Armitage, B. A. *Org. Lett.* **2008**, *10*, 1561. Sando, S.; Narita, A.; Hayami, M.; Aoyama, Y. *Chem. Commun.* **2008**, 3858. Lee, J.; Lee, K. H.; Jeon, J.; Dragulescu-Andrasi, A.; Xiao, F.; Rao, J. *ACS Chem. Biol.* **2010**, *5*, 1065.